SAND REPORT
SAND2002-3988
Unlimited Release
Printed December 2002

New Architectures for Micro-Total-Analytical Systems

Paul C. Galambos, Arthur E. Pontau, Murat Okandan, Conrad D. James, Brian J. Kirby, Timothy J. Shepodd, Kenneth R. Pohl, Seethambal S. Mani

Prepared by
Sandia National Laboratories
Albuquerque, New Mexico 87185 and Livermore, California 94550

Sandia is a multiprogram laboratory operated by Sandia Corporation,
a Lockheed Martin Company, for the United States Department of Energy's
National Nuclear Security Administration under Contract DE-AC04-94-AL85000.

Issued by Sandia National Laboratories, operated for the United States Department of Energy by Sandia Corporation.

Available to DOE and DOE contractors from
U.S. Department of Energy
Office of Scientific and Technical Information
P.O. Box 62
Oak Ridge, TN 37831

Telephone: (865)576-8401
Facsimile: (865)576-5728
E-Mail: reports@adonis.osti.gov
Online ordering: http://www.doe.gov/bridge

Available to the public from
U.S. Department of Commerce
National Technical Information Service
5285 Port Royal Rd
Springfield, VA 22161

Telephone: (800)553-6847
Facsimile: (703)605-6900
E-Mail: orders@ntis.fedworld.gov
Online order: http://www.ntis.gov/help/ordermethods.asp?loc=7-4-0#online

Final LDRD Report
for
New Architectures for Micro-Total-Analytical Systems
(project 10756)

Introduction:

The goal of this LDRD was to develop new architectures (technologies, devices and techniques) that could enable μHPLC (Microfabricated High Performance Liquid Chromatograhy) by utilizing Sandia National Laboratories' unique capabilities in the areas of EKP (Electro-Kinetic Pumping) and microfabrication. We were not intending to develop a μHPLC system, but rather components useful to such a system. There were significant personnel changes during this project, as evidenced by the fact that there were 5 different PI's over the course of the 3-year LDRD. Despite this turnover, or perhaps because of it, we have been successful in demonstrating of a wide range of different technologies, devices, and techniques with potential applicability in a μHPLC system. This project has been broad and varied rather than narrow and concentrated in scope. As such the capabilities demonstrated read like a list of different technologies, devices, and methodologies potentially useful in many microfluidic systems. The common theme of this list is the utilization of electrokinetic flow phenomena in microfabricated microfluidic systems.

This project contributed to the development of the following new technologies, devices and techniques that utilize electrokinetic phenomena in microfabricated structures:

1) Bead packed glass flow channels with integrated metal electrodes for EKP. On-chip electrokinetic pumps in glass were fabricated and tested. A theory describing flow through these pumps was developed.
2) An on-chip sample injection technique was developed for use in the glass EKP channels described above.
3) Porous polymer plugs fabricated within microchannels. In channel actuatable plug valves were fabricated and characterized.
4) Integrated surface micromachined silicon nitride channels with built-in electrodes for on-chip electrokinetic flow systems. Electrokinetic pumps and dielectrophoretic concentration and separation systems were fabricated and tested.
5) Combined, highly integrated glass/silicon microfluidic systems containing electrokinetic pumps. These hybrid systems were connected using an anodic bonding technique to join the silicon die containing electrokinetic pumps to a glass flow manifold. Initial testing of flow in the hybrid microfluidic systems was conducted.
6) The use of Zwitterionic additives to improve EKP performance was demonstrated.

The remainder of this report will consist of a discussion of each of the items on this list.

1.0 Bead packed glass flow channel EKP

Bead packed glass EKP channels with integrated metal electrodes. Please provide images of channels and representative data (e.g. pressures and flow rates developed, pump curves). Also, please describe the theory developed to quantify flow through these packed channels. **(Tim Shepodd, Brian Kirby)**

2.0 On-chip sample injection.

The 3rd figure in the LDRD renewal for the 1st year (01-1329) shows an on-chip EKP with a sample injector. Please expand on this figure. Also, it is stated in the 01 report that there will be pressure injector designs and that characterization of these designs will be accomplished. Was this ever done and can we include some of these results? **(Tim Shepodd, Brian Kirby)**.

3.0 Porous polymer plugs.

Please provide images of plugs in channels description of how they are fabricated and some representative data concerning their use as fluid switches or valves (e.g. switching times or video). **(Tim Shepodd, Brian Kirby)**

4.0 Integrated surface micromachined silicon nitride channels with built-in polysilicon electrodes.

Describe the fabrication process for SwIFT and how it was used to create channels containing built-in electrodes as they are applied to dielectrophoretic concentration/separation devices, and on-silicon EKP's. Describe the design of these devices and simple representative calculations as to how they should work.

a. Describe characterization of dielectrophoretic separations using beads.
b. Describe silicon EKP characterization.

(Paul Galambos, Murat Okandan, Conrad James)

5.0 Glass/silicon hybrid microfluidic systems.

Describe fabrication of the glass flow manifold. Describe how hybrid glass/silicon devices are assembled using anodic bonding fixture and associated methodology. Describe initial characterization of these devices. **(Paul Galambos, Murat Okandan, Conrad James)**

6.0 Zwitterionic additives to improve EKP performance.

Describe work to improve efficiency of EKP's using controlled pH. **(Brian Kirby)**

4.0 Silicon nitride channels with built-in polysilicon electrodes.

The primary goal of this LDRD was to develop microfabricated architectures for microfluidic systems utilize electrokinetic phenomena. A potentially promising architecture uses surface micromachining to make shallow flow channels on top of wafers. The starting wafers are typically, but not always, made from silicon – the same starting substrate used for IC (integrated circuit) manufacturing. Surface micrmachining allows one to use the extensive tool set that has been developed for CMOS processing (IC's) to microfabricate devices and systems on-chip. We have developed surface micromachining extensively for use in our MEMS (Micro-Electro-Mechanical Systems) process (SUMMiT^{TM} – Sandia Ultra-planar Micro-Machining Technology) **(need reference)**. Therefore a goal of this LDRD was to use our surface micromachining process to make on-silicon electrokinetic flow structures (channels with built-in electrodes), in particular electrokinetic pumping, separation, and concentration devices.

The factors that make surface micromachined architectures potentially attractive for electrokinetic systems include batch fabrication, on-chip integration of electrokinetics with MEMS and CMOS, and fine feature size definition in all 3 dimensions. Batch fabrication allows production level quantities of Microsystems to be fabricated simultaneously for costs comparable to those for IC production. The well-developed infrastructure and tool set of the IC industry can be utilized to efficiently mass-produce electrokinetic devices. This is the same argument used for surface micromachined MEMS. While we have yet to see the MEMS market explode the way the IC market has, there are niche applications where batch fabricated mass-produced MEMS has been successfully applied (e.g. airbag accelerometers – **need reference**). The same type of market impact is probably possible with surface micromachined electrokinetic systems. They can be batch-fabricated relatively cheaply to satisfy needs in specific niche markets. The issue becomes what are these niche markets and what volume of production is required to fill these niches? Is the volume of production large enough to justify the initial high capital (and time and talent) costs associated with setting up a batch

fabrication facility dedicated to electrokinetic devices? A facility that is flexible enough to be used to fabricate electrokinetic devices as well as MEMS devices would have a better chance of being justified economically as it could be used to make a wide range of products.

There is a niche market associated with electrokinetics already in existence. This market is centered around using electrophoresis to separate DNA and other chemicals of interest into bands along channels for very small volume chemical analysis systems **(need reference – Oak Ridge Boys)**. These on-chip electrophoresis systems are being used as high throughput analysis tools in the bio-tech industry (**need reference** caliper web site and other refs.). Typically these devices are etched into glass and the electrical fields are applied using electrodes at the inlet and exit of the glass channel to drive the sample through the channel and separate constituents based on their charge/mass ratio. To reduce cost some manufacturers have changed from glass to plastics (e.g. acrylic or polycarbonate) as the material of choice for their electrokinetic systems (**need reference** Tony Ricco's company presentation at Transducers and/or MicroTAS). In either case (glass or plastic) the field is generally applied at the ends of the microfabricated channels and relatively high voltages are applied. Elsewhere in this report we report on efforts to incorporate metal electrodes into glass channels to reduce the voltage required to produce the desired electrokinetic flow phenomena. Electrokinetic phenomena are field not just voltage dependent.

Even though silicon batch fabrication is relatively inexpensive (depending on batch size) it is hard to envision how this fabrication technique can compete with plastic molding or embossing in terms of cost. Therefore it must present other advantages to be considered a viable technology vis a vis plastic fabrication. One clear advantage that surface micromachining has over plastics, and any other fabrication technology for that matter, is integratability. Using various techniques (reference Montague) electronics can be integrated with MEMS on a single monolithic piece of silicon, thereby reducing assembly requirements, parasitic losses and fabrication costs while providing a highly integrated multifunctional platform for a wide range of niche applications such as DNA manipulation, cell sorting and/or concentrating, and electro-osmotic pumping. In

addition we have been able to show that MEMS can be integrated with microfluidics (**need reference** - cell-masher and cell-masher figure). Therefore it should be possible to integrate MEMS, microfluidics and electronics with chemical sensing and biological elements on a single monolithic silicon substrate. Such a substrate would provide a highly integrated platform for nanotechnology as well addressing the niche Microsystems needs just mentioned. Certainly it provides a much higher level of integration, complexity, and functionality than a piece of plastic containing a flow channel.

Another important factor that makes surface micromachined electrokinetics attractive is the ability to define local structures very precisely in all three dimensions. In the x-y plane structures are definable to the photolithographic limit of less than 1 μm, while in the z (vertical – up from the wafer) gaps between layers and layer thickness can be defined to the resolution of the CVD (Chemical Vapor Deposition) processes used to lay down the films **(a few nanometers – Is this correct?)**. In the on-silicon EKP's that will be described shortly this capability was used to define channel depths of 0.1 and 0.3 μms that are in-effect the pore size for these pumps. The precision in x-y feature definition allows us to place electrodes at any arbitrary location in channels simply by defining a doped polysilicon structure as an electrical signal line. This powerful feature means that we can apply extremely high fields with relatively low voltages simply by placing the electrodes across which the field is applied very close to each other in the channels. Relatively large electrokinetic effects can be generated with relatively small voltages.

These advantages of surface micromachining are balanced by obstacles that must be overcome in order to reap the benefits described above. These obstacles are; the conductive nature of the polysilicon used in the SUMMiT^{TM} process, the fact the polysilicon is opaque, and difficulty in packaging and filling the very small microfluidic channels that result from surface micromachining. To make surface micromachined electrokinetic devices on-silicon we need insulated channels in which electrodes are defined. To accomplish this we have modified the SUMMiT^{TM} process by adding low stress silicon nitride layers to the SUMMiT^{TM} film stack. The modified SUMMiT^{TM} process is known as SwIFT^{TM} (SUMMiT^{TM} with Integrate Fluidics Technology). The

new silicon nitride layers become the insulated channel walls, while the polysilicon layers are used as electrical signal traces and embedded in-wall electrodes. By cutting the silicon nitride walls at locations where polysilicon electrodes are defined we can place electrodes in direct contact with the liquid in the channel. The film stack used in the SwIFT™ process is shown in Fig. 1.

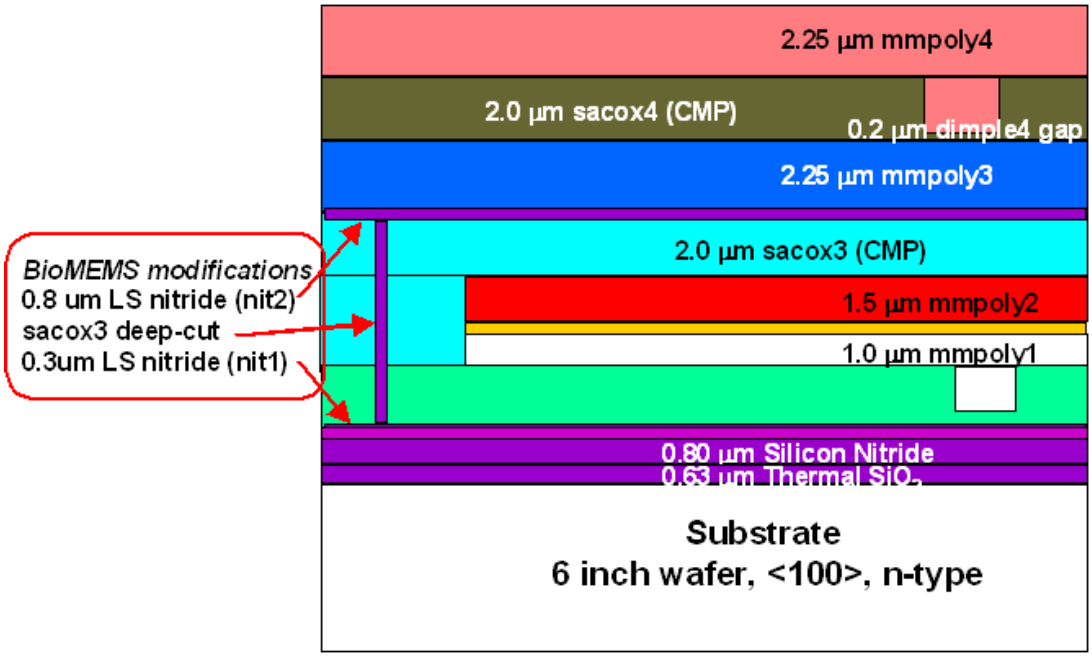

Figure 1. Additional silicon nitride layers added to the SUMMiT™ film stack (BioMEMS modifications in the image above) to create the SwIFT™ process, allow us to fabricate surface micromachined on-silicon electrokinetic devices.

Several additional advantages accrue from the BioMEMS modifications used in SwIFT™. The silicon nitride is optically transparent allowing us to see into the channels. This allows us to image particles as they are manipulated electrokinetically (electrophoresis and dielectrophoresis) by the in-channel electrical fields. Also, the mmpoly1 and mmpoly2 layers (polysilicon) in the figure allow us to place moving mechanical structures inside the silicon nitride channels. The combined electrical, optical and mechanical access available with this technology provides unprecedented

microsystem integration opportunities. Figure 2 shows a cellular manipulation device built using the SwIFT^{TM} technology. In-channel electrodes and an in–channel mechanical device are both clearly visible. Figure 3 shows a close up of the electrical trace definition using polysilicon layers.

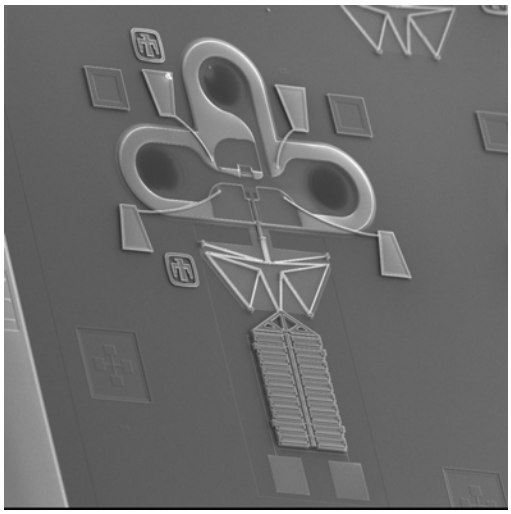

(a)

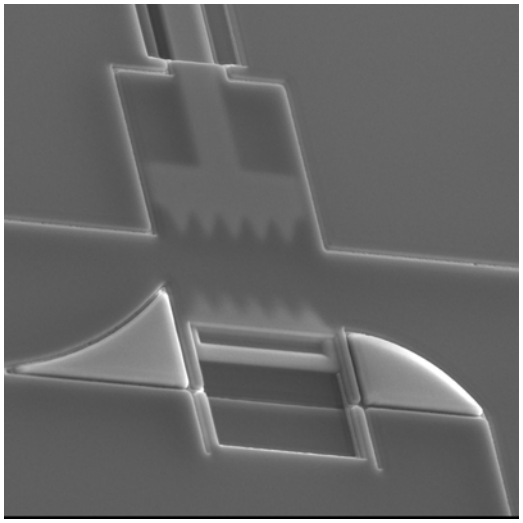

(b)

Figure 2. Cellular transfection device fabricated using the SwIFT^{TM} process: (a) shows fluid entrance and exit ports Bosch etched from the back side of the wafer, the out of channel electrostatic actuator, and the bond pads for electrical connections with conducting traces; (b) shows the actuated mechanical structure in the channel as seen through the silicon nitride channel cover.

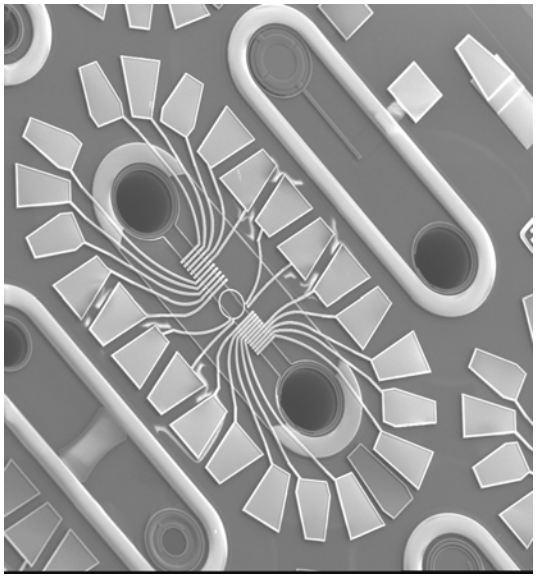

(a)

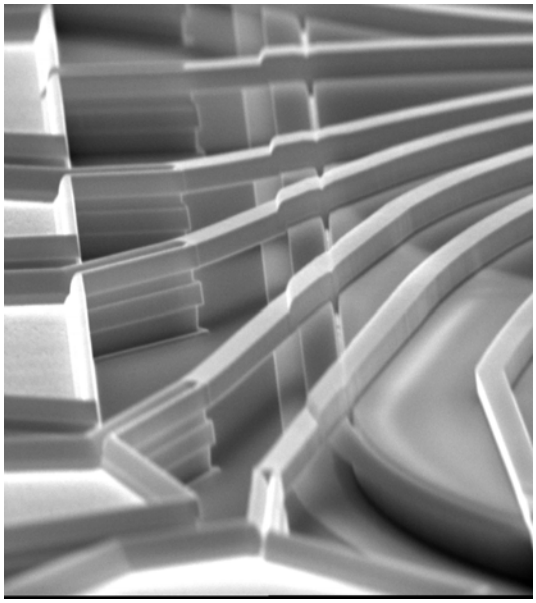

(b)

Figure 3. Electrical trace definition using polysilicon structures in SwIFT^{TM}: (a) shows bond pads and electrical traces surrounding a silicon nitride channel and (b) is a close up of an mmpoly3 (polysilicon) trace on top of the silicon nitride channel.

SwIFT™ Dielectrophoretic Particle Separation/Concentration

We tested two specific sets of SwIFT™ designs that are pertinent to this LDRD. The first set of designs are on-chip dielectrophoretic particle manipulation devices. The specific device that was most effective utilized exposed electrodes (current flow directly into liquid). Figure 4 is taken from the AutoCAD file used to design the devices and Figure 5 is a cross-section of the design generated using our cross-section visualizer.

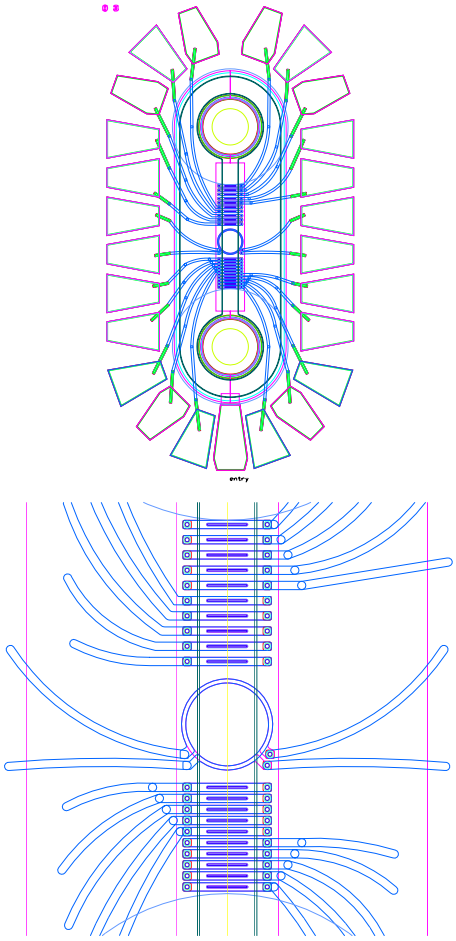

Figure 4. AutoCAD images of SwIFT™ dielectrophoretic channels: top view shows channel entrance and exit, bond pads for electrical signal application, and polysilicon electrical traces; (bottom) closeup of section containing electrodes inside of channel. The center ring electrode is not in direct contact with the liquid in the

channel while the upper and lower line electrodes are in contact with the liquid in the channel through cuts in the top nitride.

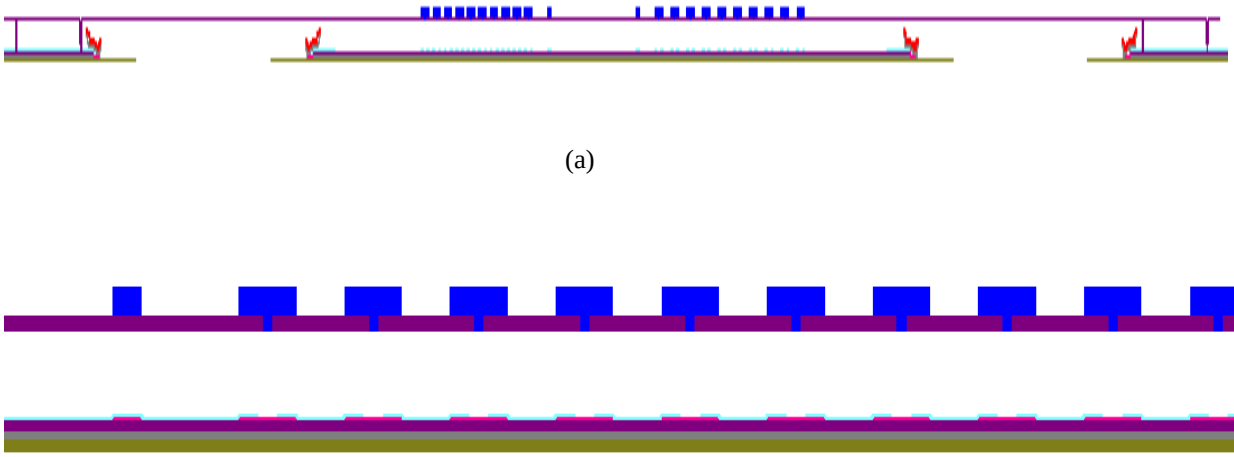

(a)

(b)

Figure 5. Cross-sections of dielectrophoretic concentration and separation devices: (a) wide view showing inlet and exit holes and electrode section, (b) close-up of electrode section. Note the cuts in the insulating silicon nitride that allow direct electrical contact to the liquid on both the top and bottom of the channel. Poly0 (bottom polysilicon layer – typically used to route signals) is magenta and Poly3 top electrodes are dark blue.

The device shown in Figs. 4 and 5 was used to separate and concentrate different particles in the channel using an AC signal applied to two of the in-channel electrodes to induce dielectrophoretic effects on the particles. Dielectrophoresis (DEP) is a phenomenon in which non-uniform electric fields (both AC and DC) induce forces on molecules, particles, and cells. The steady-state force generated on a particle of radius r_p by an electric field $\vec{E}$ is:

$$\left\langle \vec{F}_{DEP} \right\rangle = 2\pi\, r_p^3 \varepsilon_f \,\mathrm{Re}\left[\frac{\varepsilon_p^{\,*} - \varepsilon_f^{\,*}}{\varepsilon_p^{\,*} + 2\varepsilon_f^{\,*}} \right] \vec{\nabla} \vec{E}^{\,2}_{rms} = 2\pi r_p^3 \varepsilon_f \,\mathrm{Re}\left[K^*_e \right] \vec{\nabla} \vec{E}^{\,2}_{rms} \qquad \text{Eq. 1}$$

where ε^*_p and ε^*_f are the complex permittivities of the particle and the fluid, respectively, and K^*_e is the Clausius-Mossotti factor. According to Eq. 1, particles are attracted to regions of large $\vec{\nabla}\vec{E}^2_{rms}$ if Re[K^*_e] > 0 (positive DEP), and repelled if Re[K^*_e] < 0 (negative DEP). Figure 6 shows the microchannel filled with a solution of 1:4 isopropanol:deionized water that contains 1 μm diameter latex beads. After application of an AC voltage of 10 V p-p at 30 MHz between two polysilicon microelectrodes, the latex beads are repelled by a negative DEP force.

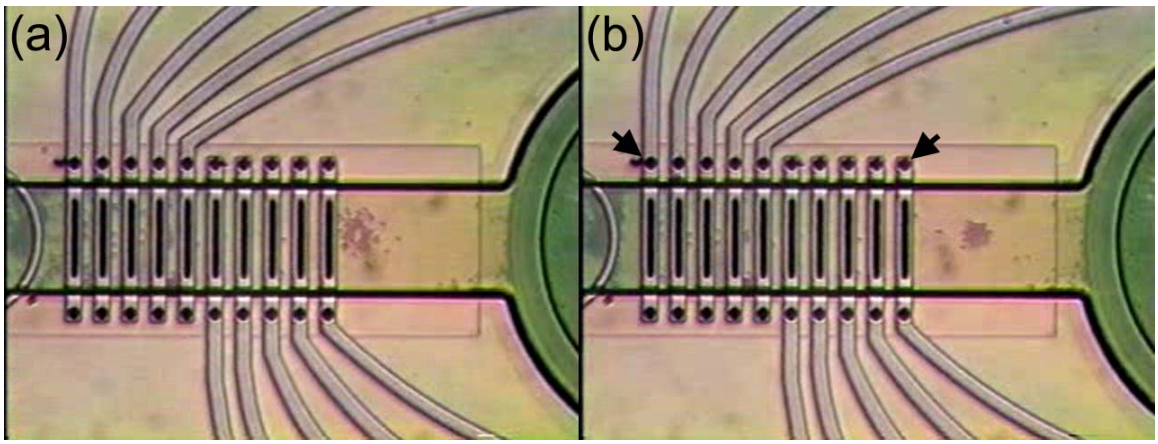

Figure 6: Dielectrophoretic manipulation of latex beads within a surface micromachined microfluidic channel. (a) At time t=0, there is no electric field present and beads are randomly distributed in the channel. At t = 0^+, a 10 V p-p, 30 MHz voltage is applied between the two microelectrodes indicated in (b). (b) At t = 4.5 seconds, the latex beads have been repelled ~20 μm from the microelectrode and concentrated into a small volume.

Figure 7 shows the same device with potentiated microelectrodes with the same field described previously. In this instance, a fluid flow is being applied in one direction. A population of beads can be seen adjacent to one of the microelectrodes, being repelled by negative DEP and withstanding the fluid flow. We envision using such a device for separation/filtering of populations of analytes (such as particles, cells, and molecules).

Due to inherent differences in the frequency-dependent complex permittivities of different analytes, variation of the frequency and magnitude of the applied electric field can be used to select for a particular analyte and concentrate that analyte from a heterogeneous mixture (e.g., selecting for white blood cells in a saliva sample).

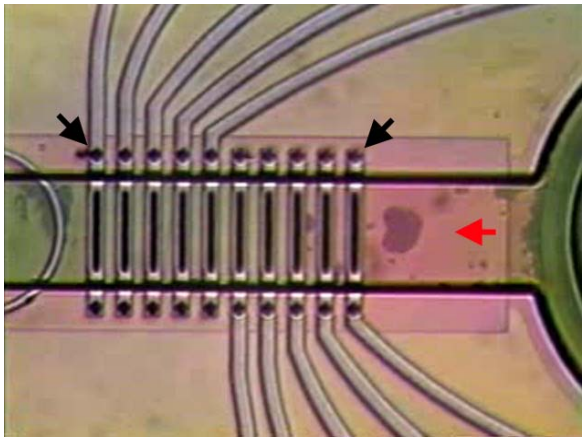

Figure 7: Negative dielectrophoresis of latex beads under fluid flow. In the presence of a steady fluid flow of ~25 μm/s (red arrow), a population of beads is repelled from potentiated microelectrodes (black arrows, 10 V p-p, 30 MHz) and is concentrated near the upstream electrode.

These initial demonstration experiments show that SwIFT^{TM} devices can be used to apply electric fields to fluids in channels and that these fields can be used to manipulate particles in solution. The highly integrated architecture of these on-silicon devices should allow them to be used to manipulate cells in on-chip microfluidic Microsystems. While not an idea electrode material (e.g. platinum) the polysilicon was adequate to deliver the field to the liquid and the silicon nitride layers provided an effective insulating film.

SwIFT™ Electro-osmotic Pump

A second set of on-silicon electrokinetic devices built using the SwIFT™ process were electrokinetic pumps. The silicon nitride EKP's that have been built on this LDRD are to our knowledge the first on-silicon EKP's that have been demonstrated.

These pumps utilized a very thin oxide deposition to make the gap between the bottom and top surfaces of the pump channel very narrow. We fabricated 0.1 and 0.3 μm deep channels in this manner. The channel walls are low stress silicon nitride. An image taken from the AutoCAD design of typical on-silicon pumps are shown in the following Figure (Figure 8).

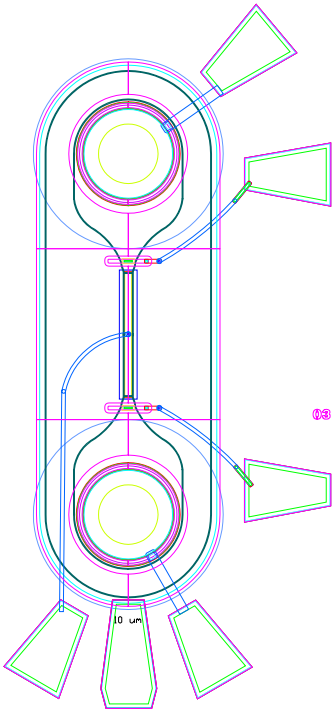

Figure 8. AutoCAD design of SwIFT™ surface micromachined silicon nitride pump. Pump inlet and outlet - circles at the top and bottom of the figure. Thin section between inlet and outlet is the pump channel. Bond pads and polysilicon electrical 'lines' allow field to be applied around the inlet and outlet holes, on a

polysilicon pad just outside the pump channel in the center of the pump and at two posts just on either side of the pump channel.

A cross-section taken through the centerline of the pump from top to bottom (Fig. 8) is shown in Figure 9. We are able to take these cross-sections of AutoCAD designs using our cross-sectional visualization tool (**need reference**). The cross sections show the very shallow pump channel (0.3 microns deep in this case) in the center section of the device and the locations where fields can be applied so that there is direct contact with the liquid.

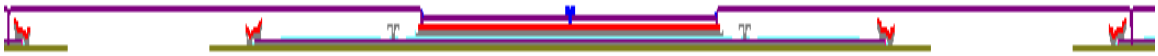

(a)

Figure 9(a). Cross-section down centerline of the pump. The vertical dimension has been greatly expanded in order to see the very thin channel. Channel inlet and exit at each end. Electrode posts just on each side of the thin pump channel section. Top poly3 (3rd polysilicon film - dark blue) electrode connects to outside of pump channel polysilicon strip in the center of the device.

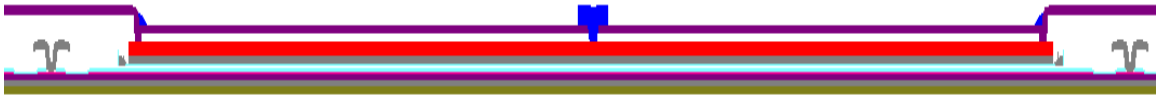

(b)

Figure 9(b). Close up of pump channel cross-section. The vertical section is again greatly expanded to aid in channel cross-section visualization. Red and gray polysilicon layers are poly1 and poly2 respectively and the combined poly1/poly2 structure in the center of the channel is used to apply a field on the outside of the channel. Electrode posts are shown at each end of pump channel (gray – poly1). The channel silicon nitride cover and bottom silicon nitride insulation are purple. Pump channel silicon nitride lining is light blue.

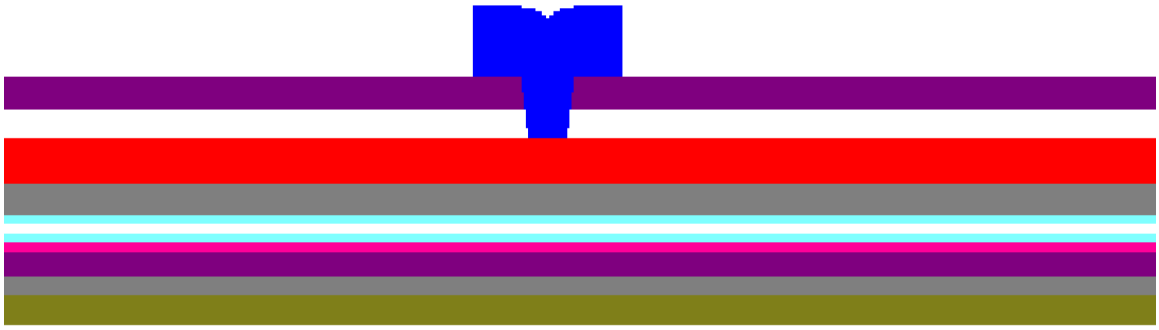

Figure 9c. Extreme close-up of the center of the channel. Again the vertical dimension has been greatly expanded so that we can see the channel. The surface micromachined films from bottom to top are: silicon wafer (olive green), bottom insulating oxide (gray), bottom insulating nitride (protects oxide during release process, purple), poly0 – bottom electrical trace (magenta), bottom of channel silicon nitride insulation (light blue), channel (white), top of channel silicon nitride insulation (light blue), poly1/poly2 combined outer electrode (gray – poly1, red – poly2), trapped oxide (white), top silicon nitride (nitride 2 – purple), poly3 electrode (dark blue). The channel depth (between 2 light blue nitride layers) is 0.3 μm.

The electrokinetic pump works because of electro-osmosis (a bulk fluid electrokinetic flow phenomena). A double-layer of charge builds up on the insulating channel walls, in this case low stress silicon nitride. An electric field is applied along the length of the channel. In the figure above (Fig. 9b) a potential could be applied at one of the end posts while the other post is grounded. The field along the channel acts to drive the charged fluid near the channel walls through the channel. The charged fluid near the wall (double layer) drags the rest of the fluid in the channel along with it due to viscous effects. The fact that the channel is so shallow makes this affect the dominant pumping mechanism to move fluid down the channel. The velocity profile for electro-osmotic flow is typically a uniform plug velocity across the channel. Simple relationships describing electro-osmotic flow have been developed at Sandia National Laboratories and elsewhere **(need a couple of references).** Since the velocity profile is uniform across the channel, a calculation of the velocity allows the flow rate to be determined. As derived in (**need reference** _) the electro-osmotic velocity can be calculated from:

$$V_x = \left(\frac{\zeta \cdot \varepsilon}{\mu} \right) \cdot E_x \qquad \text{Eq. 2}$$

where V_x is the electro-osmotic velocity along the channel, E_x is the field along the channel (voltage drop between electrodes divided by the distance between electrodes), μ is the fluid viscosity, ε is the liquid dielectric, and ζ is the zeta potential at the walls. This relation assumes that there is no overlap in double layers from each wall and provides a simple order of magnitude accuracy method for predicting pumped fluid velocity for a given applied field.

Using Eq. 2 we can calculate a typical electro-osmotic velocity for our channel designs (Fig. 9 above). Using water as the working fluid: $\mu = 10^{-3}$ N-s / m^2, and $\varepsilon = 80 \times 8.854 \times 10^{-12} = 7.08 \times 10^{-10}$ C^2 / N-m^2. The value of zeta potential (a measure of the charge or potential built up in the double layer along the insulated channel wall) was taken from the literature from measurements of streaming potential in buffered aqueous solutions along similar low-stress silicon nitride insulating walls **(reference)**: ζ = -40 mV at pH 7. Lets assume a low voltage of 10 V is used across the approximately 500 μm long EKP channel with a resulting field strength of 2×10^4 V/m. Note that even though the voltage used is relatively low the field strength is relatively high due to the short distance between electrodes. Using these values in Eq. 2 an electro-osmotic velocity of $V_x = 5.7 \times 10^{-4}$ m/s is predicted in the pump channel. The pump channel cross-section is 0.3 μm by 13 μm with an area of 3.9×10^{-12} m^2. Therefore the flow rate predicted is $5.7 \times 10^{-4} \times 3.9 \times 10^{-12} = 2.2 \times 10^{-15}$ m^3 / s (2.2 pl / s).

If the outlet of the channel is plugged pressure will build up at the plugged end and fluid will travel towards the plugged end near the channel walls (driven by electro-osmotic flow) and away from the plugged end (towards the channel inlet) in the center of the channel (driven by pressure). The net flow rate will be zero and a large pressure can be generated in the plugged channel. Sandia National Laboratories researchers have generated pressures > 10,000 psi in packed capillary EKP's (**reference**). Eq. 2 above

assumes that the channel is completely unplugged and that there is no pressure drop along the channel.

An experiment to demonstrate whether electro-osmotic pumping was being achieved in the device described above was conducted. A buffered aqueous solution (pH 7 – check this) was loaded into the on-silicon EKP through a glass flow manifold. The glass manifold, the attachment of the silicon die to the glass manifold and the filling of solution into the glass manifold will be described later in this report. It was determined that the pump channel was filled with liquid optically through the transparent nitride cover and by viewing the liquid/gas meniscus in the transparent glass channel downstream of the on-silicon channel. We also were able to determine that current was getting from the powered probe tips to the in-channel electrodes through the polysilicon bond pad and trace. When a voltage greater than approximately 20 V DC was applied to the bond pads and therefore to the in-channel electrodes through the polysilicon trace (Fig. 8) a gas bubble was observed to form at the electrode surface in the channel. The electrodes used in this test and in the pumping demonstration to be described shortly were the ring electrodes that surround the inlet and exit channel holes (see Fig. 8). The gas bubbles generated at the electrodes were due to electrolysis. Cycling the voltage by turning power on and off resulted in gas generation when power was turned on and gas bubble collapse when power was turned off, clearly establishing the electrical connection to the liquid in the channel.

The electrolysis voltage also sets an upper limit on voltage that can be used with this aqueous solution to generate electro-osmotic flow. At voltages greater than approximately 20 V gas bubble generation effectively limits current flow through the liquid and therefore limits the ability of the electro-osmotic pump to move fluid. In this case current flow and liquid flow are two aspects of the same physical phenomena, the movement of an electrically charges fluid through a channel. The 20 V limit is higher than expected since for an ideal electrode only 1 to 2 V is required for electrolysis. We expect that electrolysis is occurring at lower voltages but that it is not extensive enough for significant gas generation that would stop the pump. Another factor that contributes

to the higher than expected gas generation voltage is that the fluid is moving, so that it tends to take the generated gas in solution along with it and reduce the concentration of dissolved gas at the electrode. A third factor that increases the voltage at which significant electrolysis (gas generation) occurs is the native oxide that forms on the surface of the polysilicon electrode. Experience on another project **(Xerox CRADA - reference electrochemistry paper)** indicates that some portion of the voltage is dropped across this oxide and that some anodization (oxide growth) occurs. This oxide growth is not significant enough to prevent the device from pumping, but it does result in higher than expected voltages at the bond pads for a given response at the electrode in the channel.

Even an upper limit of 20 V is lower than we would like for a high performance (high flow rate and pressure) pump. Typically in our MEMS systems we are able to apply 100 to 200 V to power various actuators (**references**). There are many ways that the electrolysis voltage can be extended. One way is to use a polar solvent such as acetonitrile as the pump fluid. Sandia CA has developed several high pressure pumps in this way **(references**). It is worth noting that slightly larger off-chip EKP systems are not as concerned with the phenomena of electrolysis because the voltage is applied to the liquid in a vented reservoir that allows any gas generated to escape. Also in the dielectrophoretic experiments described earlier we were less concerned with electrolysis because an AC signal was used and the electrode reactions are reversed every time polarity switches, thereby preventing build-up of any unwanted reaction by-products (gases).

We would like to stay with an aqueous solution because it allows us to determine where electrical contact is being made (by observing gas bubble generation at electrodes for voltages > 20 V) and because many fluids of particular interest in microfluidic systems are biological and therefore require an aqueous solution. Even in aqueous solutions various chemical additives can be used to increase the voltage that can be applied without gas generation. In the Xerox CRADA mentioned earlier gas generation due to electrolysis was inhibited by the addition of thiols (ethelene glycol check specifics) to the

liquid exposed to voltage. Finally electrokinetic pumping efficiencies can be significantly improved through the addition of Zwitterionic buffers as is discussed elsewhere in this report. Since our goal in these initial tests was just to demonstrate that we could pump liquid electrokinetically with an on-silicon pump and not to try to optimize pump performance, we were content to stick with water and apply voltages lower than the threshold electrolysis voltage of 20 V.

The results of our on-silicon EKP demonstration experiment are shown in Figure 10. The downstream from the pump meniscus is clearly visible in the glass manifold channel. Fig. 10(a) is an image taken just before the voltage was applied and Fig. 10(b) was taken just after the voltage was turned off. While the voltage was applied the liquid/gas interface was observed to move steadily from the position shown in Fig. 10(a) to the position shown in Fig. 10(b). A 9.8 V DC signal was applied at the exit ring electrode and the inlet ring electrode was at ground. Meniscus motion was observed away from the outlet indicating that liquid was leaving the outlet of the channel in the opposite direction from the potential gradient as predicted from the negative sign of the zeta potential. A current of approximately 2.4 nAmps was measured during pumping. The meniscus moved from the position shown in Fig 10(a) to the position shown in Fig. 10(b), a distance of 812 μm, in a little over 2 minutes (130 seconds). After the pump was turned off the meniscus moved back towards its original position, indicating that some pressure was built up during the pumping process. The meniscus appeared stationary prior to the application of voltage, indicating that at the beginning of the voltage application there was no net pressure on the fluid. Unfortunately we were not measuring pressure during voltage application. Subsequent tests had similar results although we did notice on some of these test that the pumping rate appeared to slow down over voltage application time. This again would be typical if pressure were building up in a direction opposite to electro-osmotic flow.

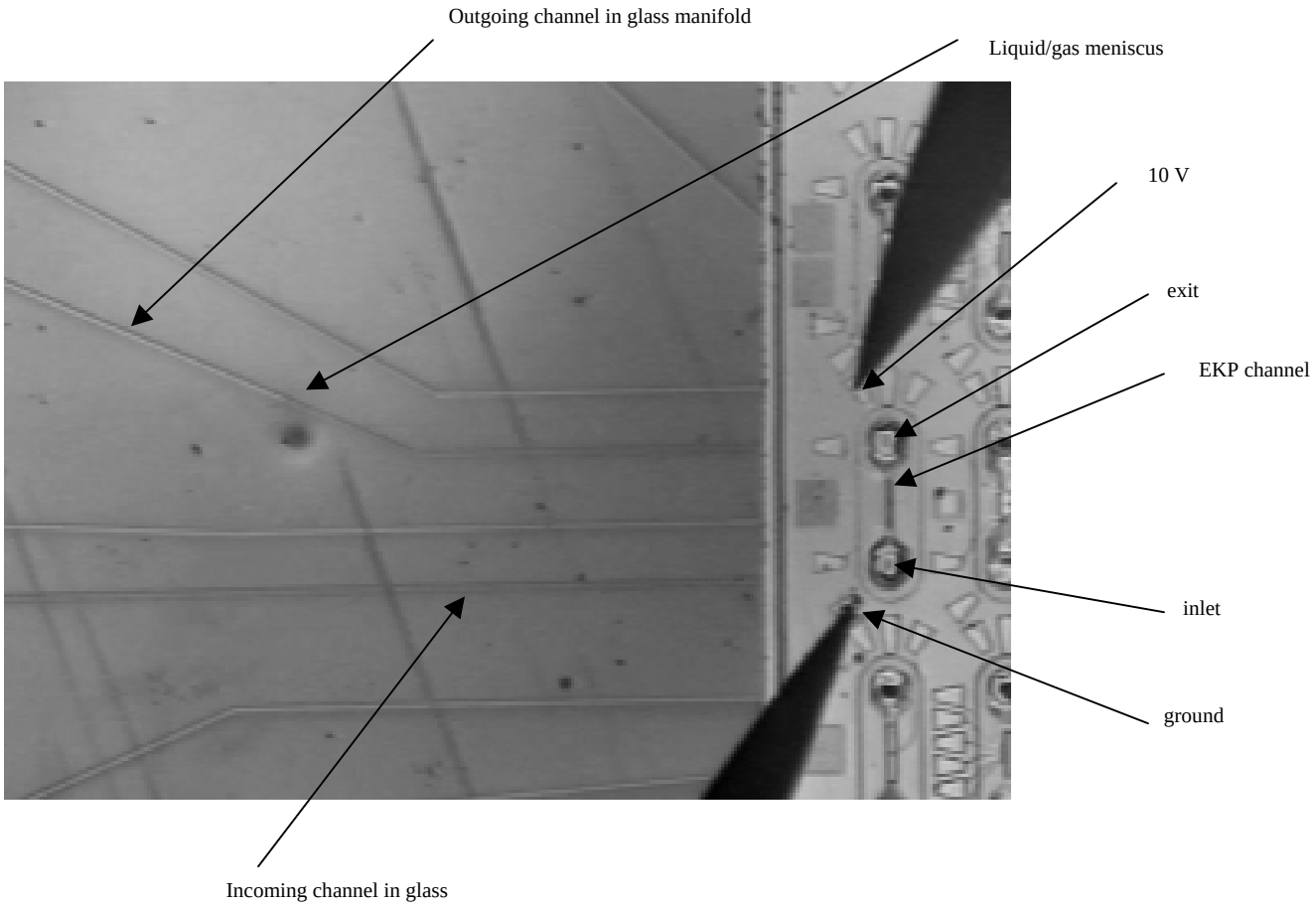

Figure 10. On-Silicon EKP – meniscus motion during voltage application: (a) before voltage, (b) after voltage (9.8 V applied for 130 seconds)

The average velocity during voltage application was 812 μm (distance traveled by the meniscus) / 130 s (time of voltage applications) = 6.24 x 10^{-6} m/s. The cross-section of the glass channel is 15 μm by 40 μm. Therefore the average flow rate measured is (15 x 10^{-6}) x (40 x 10^{-6}) x (6.24 x 10^{-6}) = 3.75 x 10^{-15} m^3/s (3.75 pl/s). This measured flow rate is in reasonable agreement with the predicted flow rate of 2.2 pl/s based on Eq. 2 (an extremely simplified model of the electro-osmotic flow phenomena). The volume flow rate remains constant for an incompressible fluid (water). As the cross-sectional area changes (for instance when the liquid leaves the very small on-chip silicon nitride channel and enters the larger glass channel) the velocity changes to compensate for the change in area and keep the flow rate constant. Therefore the flow rate in the glass channel should be the same as that in the EKP channel.

Complicating factors such as uncertainty in geometry (particularily channel depth), precise distance between electrodes, amount of double layer overlap, and the precise value of the zeta potential, make it unreasonable to expect better agreement between the measured and predicted flow rates. The measured and predicted flow rates and test conditions are summarized in Table 1.

	V_x (velocity)	Cross-section	Q (flow rate)
Measured	6.24 x 10^{-6} m/s	15 x 40 μm	3.75 pl/s
Eqn. 2	5.70 x 10^{-4} m/s	0.3 x 13 μm	2.22 pl/s

Table 1.0 Measured and predicted on-silicon EKP flow rates. In Eq. 2, E_x = 2 x 10^4 V/m (10 V over 500 μm), ζ = -40 mV, μ= 0.001 N-s/m^2, ε=7 x 10^{-10} C^2/N-m^2.

The initial experiments have verified that the on-silicon EKP can pump water at reasonable flow rates. The hard work of investigating the details of the pumping mechanism, determining optimum pumping conditions and materials, and integrating the pumps into complete on-chip and/or hybrid microfluidic system remains to be done.

5.0 Glass/silicon hybrid microfluidic systems.

Packaging very small-scale microfluidic Microsystems is a challenging task. In particular making multiple sealed microfluidic channel connections that are very tightly spaced is difficult. The SwIFT^{TM} surface micromachined microchannels are connected to the outside world through Bosch etched high aspect ratio vertical walled holes through the wafer (**need a reference**) connecting mating channels in the larger microsystem to the end of channel connecting holes (inlet and exit). There might be only on the order of 500 μm between connecting holes in the SwIFT^{TM} process. Therefore the problem resolves to one of how to make very tightly spaced sealed fluid connections to the back of a silicon die. Making individual hole connections is very difficult and time consuming at this scale, therefore it is expedient to make all the fluid connections at once when attaching the silicon chip to the larger microfluidic system. The larger microfluidic system is often a meso-scale system to which standard fluid connections (e.g. capillaries) can be made.

In this case the larger microfluidic system is a glass manifold. We chose glass because glass is the material most often used in electrokinetic microfluidic systems (**need reference**), because precisely patterned channels can be fabricated in glass, and because it allows the use of anodic bonding, which can provide a high strength sealed connections with very little contact area between surfaces. The problem is how to attach the silicon to the glass so that all the connecting microfluidic holes are precisely aligned and so that there is no cross-talk between channels (leakage from one channel to another). The hybrid glass/silicon system is shown in Fig. 11.

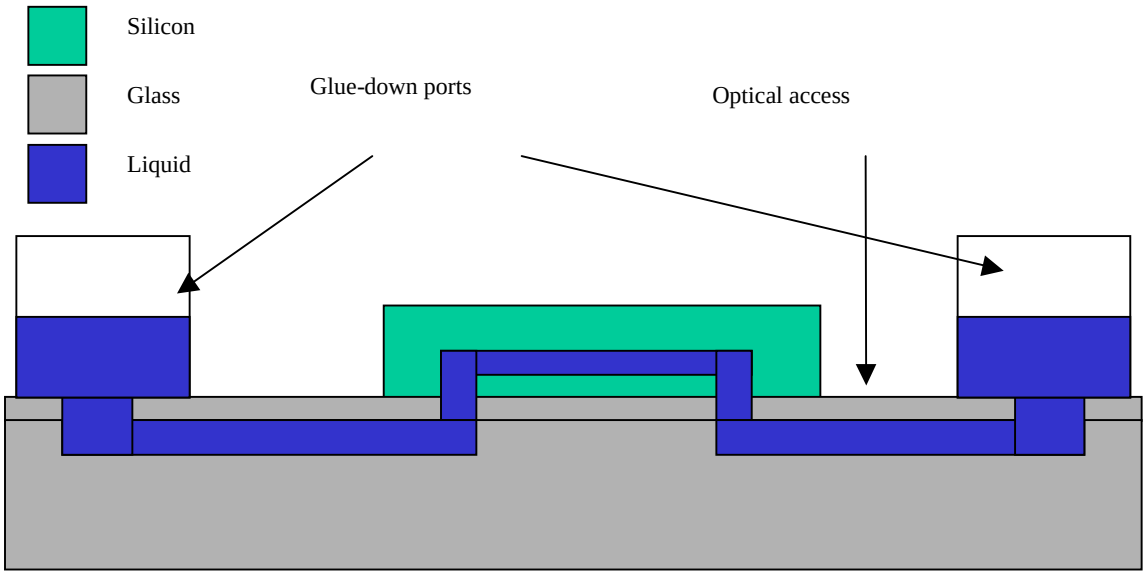

From Ron Renzi, Sandia National Laboratories

Figure 11. Hybrid glass/silicon system cross-section through a channel.

Our solution to this problem of glass/silicon hybrid assembly might be described as a relatively high expense, high quality solution. The solution utilizes a 2-layer glass flow manifold in which channels connecting to the on-silicon channels are etched. A glass cover seals the etched channels and contains holes in the precise pattern of the connecting holes on the bottom of the silicon die. The glass cover is bonded to the glass channel plate using fusion bonding (need some details of the fusion bonding process – temperature and pressure). Boro-silicate glass (boron doped) was used although Pyrex (sodium doped) would probably work better. Any p-type (**check and be sure its not n-type**) doped glass should work for this application. Although specific processing conditions would vary with glass type. The channel pattern in the glass is tightly spaced at the die connection region and spreads out and get larger in size (larger exit hole at the glass/capillary connection than at the glass/ silicon connection). Once the glass pieces were fused into a single flow manifold we were ready to attach the silicon die to the glass cover containing the matching hole pattern. The glass flow manifold is shown in Fig. 12.

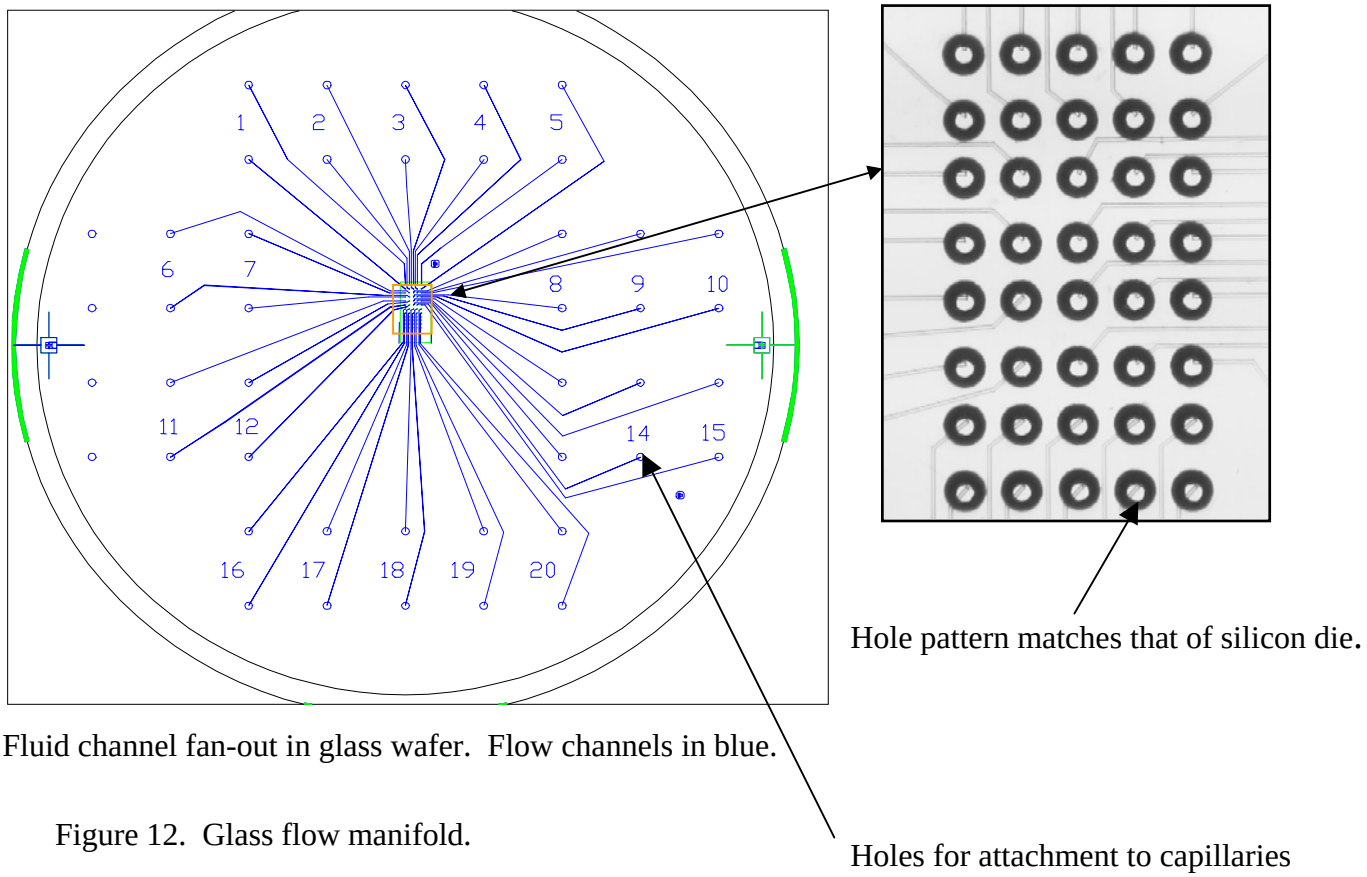

Fluid channel fan-out in glass wafer. Flow channels in blue.

Figure 12. Glass flow manifold.

Anodic bonding is an effective method of attaching silicon to glass. An anodic bond is hermetic ($<10^{-8}$ cc/s-Atm) and can provide a leak tight seal between the very closely spaced (500 μm) connecting holes. Since the holes are approximately 200 microns in diameter there are only 300 microns of material between hole edges on which to establish a seal. Other techniques, such as adhesive attachment, could potentially plug the connecting holes due to the adhesive flowing into the hole. We have also experimented with using double-sided adhesive tape (VHB tape from 3M) to attach silicon die to flow manifolds. While this can work for less tightly spaced holes where the joint does not have to withstand a significant pressure (> several atmospheres gage pressure), we have not had consistent success using the tape with higher pressures and tightly spaced connecting holes. However anodic bonding can provide an extremely strong leak tight seal with only a small area as the two materials (silicon and glass) chemically fuse to form a seamless joint that is at least as strong as either of the two materials.

Anodic bonding works in two stages, an initial electrostatic attachment between silicon and glass brings the two surfaces into intimate contact, followed by a chemical reaction at the silicon/glass interface at which a new material grows joining the two materials permanently. During the second stage of anodic bonding a silicon dioxide region forms at the interface between the silicon and the doped glass. This solid material at the interface is as strong as either of the two bonded materials and forms a gas tight connection between the materials. Unfortunately commercially available anodic bonding systems are wafer scale – not module scale. In our applications we need the flexibility to make connections to individual silicon die, therefore we require a module scale anodic bonding fixture (Fig 13).

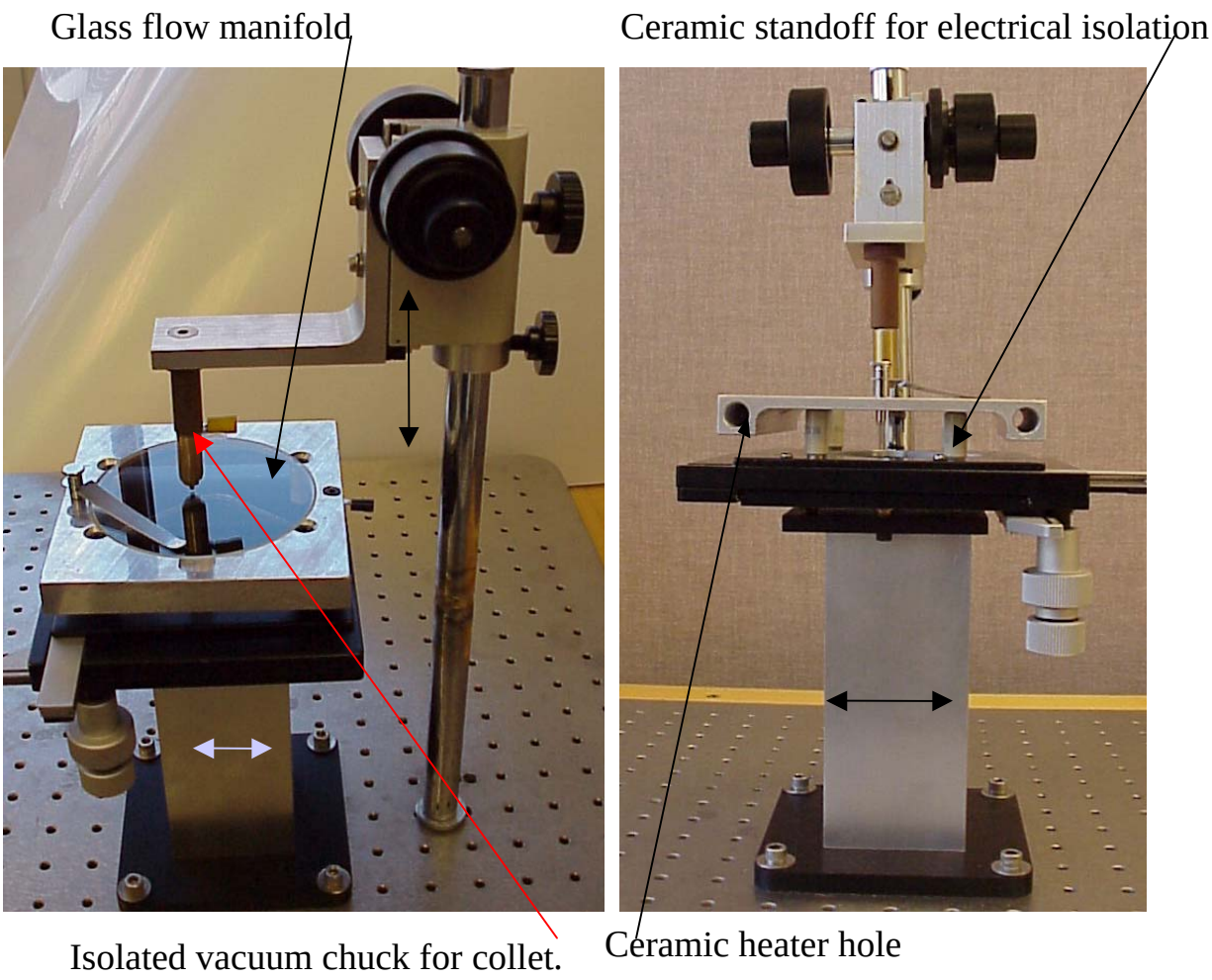

Figure 13. Anodic bonding fixture.

A close up view of the glass flow manifold on the fixture is shown in Fig. 14.

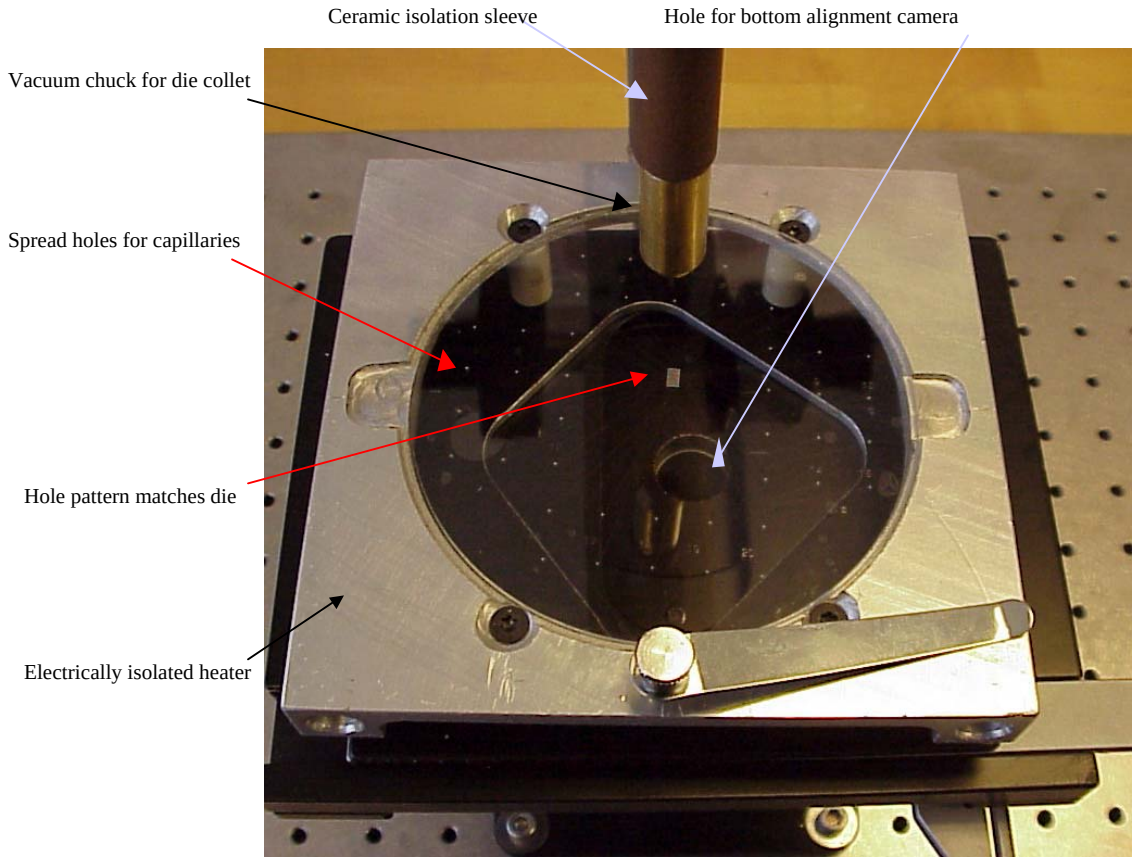

Figure 14. Close-up of glass flow manifold in anodic bonding fixture.

The anodic bonding process requires heat and high voltage. The temperature required varies from about 300 to 500 C, and the voltage required is from 1 to 3 KV. The voltage and the temperature are not independent. Generally the higher the temperature used the lower the voltage required. The high temperature acts to mobilize the charge carriers in the materials. When the voltage is applied these charge carriers move to their respective opposing charge electrodes (Fig. 15). This causes a voltage difference at the interface and a resulting electrostatic attraction between the two materials (glass and silicon). This electrostatic attraction varies as $1/d^2$, where d is the gap between the two materials. Whe the electrostatic attractive force is high enough it causes the two materials to move towards each other. This reduces d even more and in turn increases the attractive force further. Therefore below a certain gap spacing the position of the two plates is unstable and they are pulled into intimate contact (d=0) by the electrostatic attractive force.

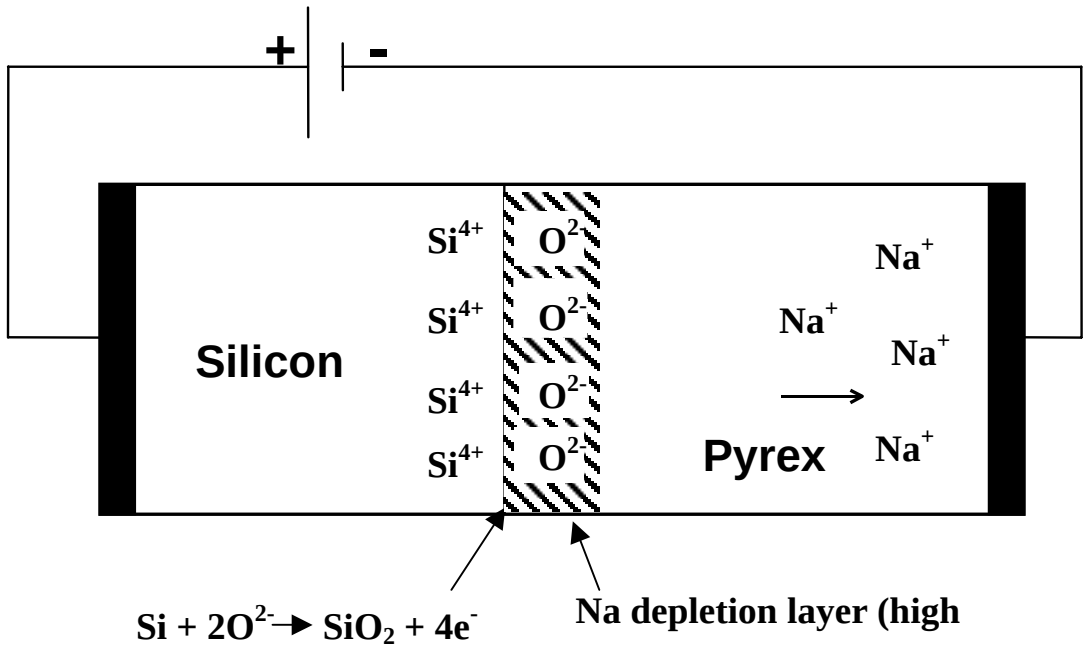

Figure 15. Anodic Bonding Process.

Once in intimate contact current flows between the materials through the interface. Associated with this current is the reaction of oxygen ions with silicon at the interface to form silicon dioxide. When a thick enough region of silicon dioxide develops the current drops and the anodic bond is complete. The interface region has in effect been anodized and the resulting silicon dioxide bridges the gap connecting the two materials with a solid crystalline structure.

The image shown in Fig. 14 is misleading in that the aluminum cover plate used during bonding is not shown. This plate covers the entire glass flow manifold except for the small region where the silicon die attaches. The cover plate attaches to the heaters as does the base plate on which the glass rests. Therefore when the cover plate is installed almost the entire glass part is enclosed and kept at a uniform temperature. The glass is electrically, but not thermally, insulated from the heaters using thin mica heat sink spacers. This prevents the AC signal used in the heater from affecting the voltage on the glass.

The hole pattern on the bottom of the silicon die is aligned to the matching hole pattern in the glass using a CCD camera and small low magnification microscope objective that is mounted beneath the glass manifold and looks up through the glass at the bottom of the silicon die. The die is held by a vacuum collet that has beveled edges that only touch the edge of the die. The surface micromachined structures on the from surface of the die are not touched or damaged by the slight vacuum. The vacuum collet is attached to a focus block that allows the die to be brought down on top of the glass. The glass manifold and heater are mounted in an x-y stage that allows the glass to be precisely positioned below the silicon die. In this system the glass grounded and the high voltage is applied to the silicon through a lug attached to the collet holding fitting.

We used the following procedure to attach the die to the glass. The silicon die is picked up using the vacuum collet and a low vacuum. The die is aligned to the glass using the vision system and then placed gently in contact with the glass using the focus block. The vacuum is then turned off to prevent any possible cooling of the die. The heater potentiostat voltage is gradually increased while the glass temperature is monitored with a thermocouple. Temperature is gradually increased until it stabilizes at the desired temperature (300-400 C typically). The heat up process takes from ½ hour to an hour. A feedback control system could be used to make the heat up a set and forget procedure.

When the temperature has stabilized the alignment is rechecked. The glass and silicon should be at approximately the same temperature. The high voltage (1-2 kV typical) is applied to the silicon die for approximately 1 hour while the glass is grounded and electrostatic attraction followed by chemical bonding occurs. Current is monitored during bonding. When the current drops off the bonding process is usually complete. The heater voltage is gradually reduced in a slow cool down process that takes an additional 1-2 hours. The process has not been optimized, but we believe that with better thermal control, optimal (lower) temperatures and higher voltages, and more highly doped glass the processing time could be reduced to under an hour. Preliminary testing with Pyrex (as opposed to the borosilicate glass used to make the manifolds) indicates that the actual bonding time (voltage on) can be reduced to < 1 minute.

Initially our fixture did not have a heater cover and was poorly positioned under an air conditioning vent. As a result we had to use higher temperatures (380 – 400 C) and the temperature on the glass was uneven. We also used only 1 kV because that was the limit of our first power supply. Due to the uneven temperature distribution we cracked several glass manifold – most often during the cool-down phase. We were, however, able to get some silicon/glass parts bonded but the resulting thermal stress led to a crack through the glass that fractured the silicon and caused it to pop off the glass (Fig. 16).

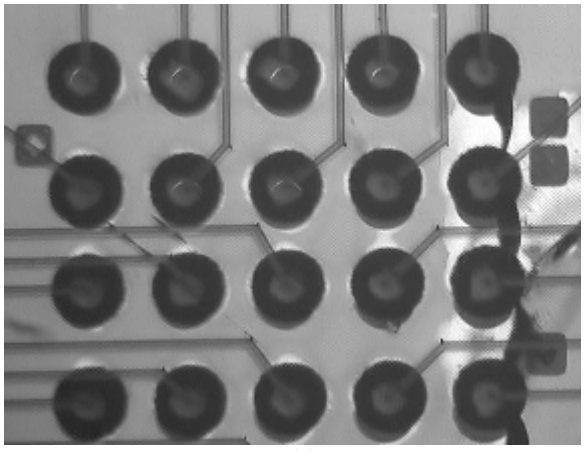

(a)

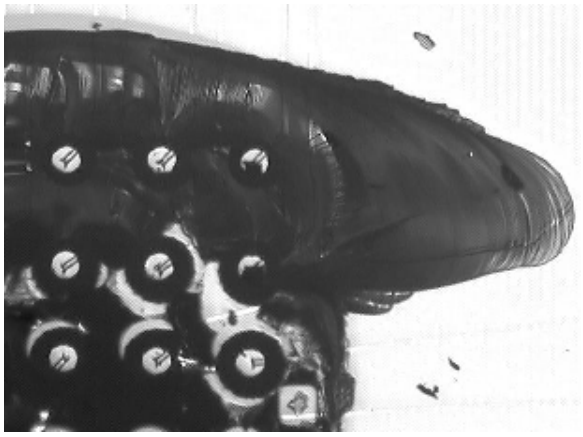

(b)

Figure 16. Failed anodic bond: (a) just after bonding (note: precise alignment between glass flow channels and holes in silicon – view through the glass), and (b) after glass/silicon structure cracked and silicon popped off.

The improvements to the fixture (more uniform temperature), change in fixture location (away from air conditioning duct), and use of a lower temperature and higher voltage (325 C and 1.5 kV) resulted of successful aligned attachment of the silicon die to the glass flow manifold (Fig. 17).

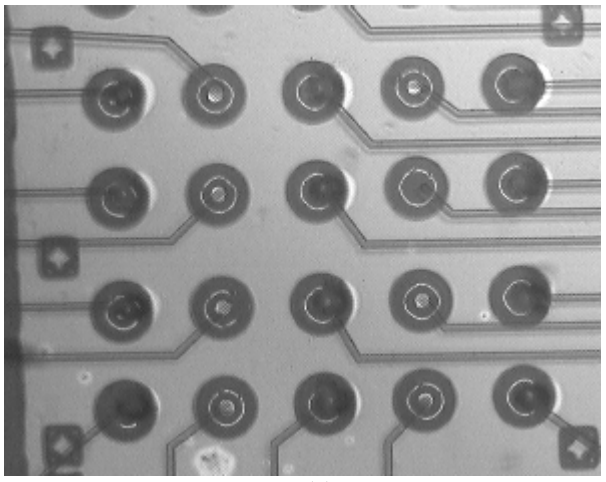

(a)

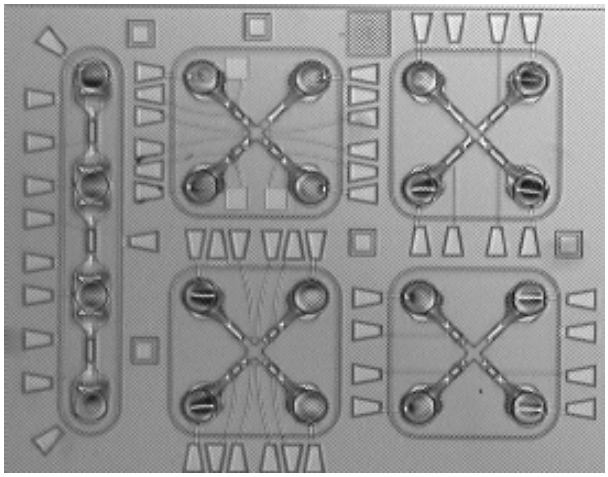

(b)

Figure 17. Successful anodic bond. Bottom view (a), Top view (b)

The ultimate proof of the attachment method was the test described earlier in this report of the on-chip EKP in which fluid connection was made through the glass manifold. To fill the surface micromachined microfluidic EKP channel anodically bonded to a glass flow manifold a specially designed fitting (Ron Renzi, Sandia National Laboratories) was

glued to the glass manifold at the appropriate entrance and exit ports. This fitting allows a capillary to be threaded into place to make a robust fluid connection with a very small volume. A drop of aqueous buffer solution was placed in the fitting well. The fitting well has a much larger volume than either the silicon or glass channels. The liquid wicked from the well into the glass channel due to capillary forces once an initially blocking air bubble was dislodged. A vacuum was then applied at the exit channel fitting. This pulled the liquid through the on-silicon channel and into the exiting glass channel. A capillary was attached to the upstream well and a syringe was used to push more fluid through the channel. Eventually we became impatient and applied too much pressure to the syringe (hoping to rapidly fill the entire exit glass channel with liquid) and cracked the thin film covering the silicon nitride EKP channel. The pressure that fractured the cover is estimated at 2-3 Atm gage pressure. During the entire test no leaks were observed anywhere in the glass manifold or in the silicon. There was no cross talk, either fluid flow or membrane cover deflection due to a pressure connection to an adjacent channel. Liquid entered the glass manifold and out the exit glass channel down stream from the on-silicon channel as it was designed to do.

In summary, in this part of the project we were able to successfully demonstrate the sealed attachment of a silicon die containing microfluidic structures to a glass flow manifold using a Sandia developed anodic bonding fixture and methodology. The hybrid glass/silicon microfluidic archtecture that was fabricated and tested, demonstrates the possibility that more complex microfluidic Microsystems can be developed in which the advantages of each substrate material can be utilized in a combined structure. For instance, controlled sample injection and electrophoretic separation could be accomplished in the glass part of the system while electrochemical sensing and dieletrophoretic particle concentration could be accomplished in the on-chip silicon nitride channels with built-in electrodes.

Distribution:

1	MS 9018	Central Technical Files, 8945-1
2	MS 0899	Technical Library, 9616
1	MS 0612	Review & Approval Desk, 9612
1	MS 0188	D. Chavez, LDRD Office, 1030
1	MS 1080	Paul Galambos, 1769
1	MS 9951	Arthur Pontau, 8358
1	MS 1080	Murat Okandan, 1749
1	MS 1080	Conrad James, 1769
1	MS 9951	Brian Kirby, 8358
1	MS 9403	Timothy Shepodd, 8722
1	MS 1080	Kenneth Pohl, 1767
1	MS 1749	Sita Mani, 1749
1	MS 9951	Duane Lindner, 8101
1	MS 9054	Bob Carling, 8350
1	MS 9004	John Vitko, 8100
1	MS 9054	Bill McLean, 8300
1	MS 9103	Jane Ann Lamph, 8111
1	MS 9951	Len Napolitano, 8100
1	MS 9951	Gabriela Chirica, 8358
1	MS 9951	Eric Cummings, 8358
1	MS 9951	Yolanda Fintschenko, 8358
1	MS 9951	Julia Fruetel, 8358
1	MS 9951	Cindy Harnett, 8358
1	MS 9951	Brent Horn, 8358
1	MS 9951	Kan Patel, 8358
1	MS 9951	Dave Reichmuth, 8358
1	MS 9951	Renee Shediac, 8358
1	MS 9951	Jay West, 8358
1	MS 9971	Boyd Wiedenman, 8358
1	MS 9951	Simon Song, 8358
1	MS 9951	Jose Cintron, 8358
1	MS 9951	Pam Caton, 8111
1	MS 9103	Bob Crocker, 8111
1	MS 9951	Bruce Mosier, 8111
1	MS 9103	Ron Renzi, 8111
1	MS 9103	Jamie Stamps, 8111
1	MS 9103	M. C. Stoddard, 8111
1	MS 9103	Karl Wally, 8111
1	MS 9103	Dan Yee, 8111
1	MS 9951	Amy Herr, 8130
1	MS 9951	Joe Schoeniger, 8130
1	MS 9951	Anup Singh, 8130
1	MS 9951	Victoria Vandernoot, 8130
1	MS 9951	Andy Walker, 8130
1	MS 9403	Linda Domeier, 8722
1	MS 9403	Blake Simmons, 8722
1	MS 1425	Steve Martin, 1701
1	MS 1425	Steve Casalnuovo, 1744
1	MS 0603	Stan Kravitz, 1763
1	MS 0603	Ron Manginell, 1764

1	MS 0603	Ron Manginell, 1764
1	MS 0892	Doug Adkins, 1764
1	MS 0958	Gil Benavides, 14184